Aerosol Science and Technology

ISSN: 0278-6826 (Print) 1521-7388 (Online) Journal homepage: http://www.tandfonline.com/loi/uast20

Novel Instrument to Separate Large Inhalable Particles

K. R. Anderson, D. Leith, M. Ndonga & J. Volckens

To cite this article: K. R. Anderson, D. Leith, M. Ndonga & J. Volckens (2015) Novel Instrument to Separate Large Inhalable Particles, Aerosol Science and Technology, 49:12, 1195-1209, DOI: 10.1080/02786826.2015.1112874

To link to this article: http://dx.doi.org/10.1080/02786826.2015.1112874

Aerosol Science and Technology, 49:1195–1209, 2015

ISSN: 0278-6826 print / 1521-7388 online
DOI: 10.1080/02786826.2015.1112874

Novel Instrument to Separate Large Inhalable Particles

K. R. Anderson,[1,2] D. Leith,[1,2,3] M. Ndonga,[1] and J. Volckens[1,2]
[1]*Department of Environmental and Radiological Health Sciences, Colorado State University, Fort Collins, Colorado, USA*
[2]*Department of Mechanical Engineering, Colorado State University, Fort Collins, Colorado, USA*
[3]*Department of Environmental Sciences and Engineering, University of North Carolina at Chapel Hill, Chapel Hill, North Carolina, USA*

Large inhalable particles are present in the workplace, yet few instruments exist to count and size such particles *in situ*. Inhalable-aerosol exposure can be evaluated using mass-based samplers such as the IOM or Button sampler, but these devices do not provide information on particle size distributions. Size-resolved samplers such as cascade impactors or the Aerodynamic Particle Sizer are limited to particle sizes <20 μm due to difficulties with particle aspiration and transmission losses. This work describes the development of two samplers capable of measuring the concentration and size distribution of airborne particles from 20 to 100 μm in aerodynamic diameter. One device is based on the principles of an upflow elutriator, whereas the other eliminates the potentially adverse effects of an upward-facing jet to separate particles from a quiescent airstream. Analytical models and computational fluid dynamics simulations were used to predict the performance of the two samplers. Sampling efficiencies of these devices were tested in a calm-air chamber with polydisperse, fluorescent microspheres (10–100 μm). Epifluorescent microscopy of settled dust was used to determine reference particle counts and sizes. Both devices are capable of size-selective sampling; however, the second sampler produced higher sampling efficiencies and sharper cut points compared to the simpler elutriator design. Experimental sampling efficiencies for both samplers showed good agreement with computational and analytical solutions. This work suggests that these devices can size-segregate inhalable aerosols in quiescent environments.

INTRODUCTION

Inhalable particles are defined as those that penetrate into the head airway region and beyond. Ogden and Birkett (Ogden and Birkett 1975) were the first to present the idea of the human head as a blunt aerosol sampler and to demonstrate that the head does not effectively inhale particles of all sizes. The inhalable particulate mass (IPM) criterion was subsequently developed to describe the fractional sampling efficiency of the human head (the inhaled fraction, or IF) as a function of particle aerodynamic diameter:

$$\mathrm{IF} = 0.5 * (1 + \exp(0.06 * d_{\mathrm{ae}}) \qquad [1]$$

for wind speeds <4 m s^{-1} and particles <100 μm (Soderholm 1989).

Exposure to inhalable aerosols is traditionally assessed using time-integrated personal samplers with gravimetric analyses to determine dust concentration (Eller and Cassinelli 1994). The 37 mm cassette is the most commonly used personal sampler in the United States for industrial hygiene sampling. However, the 37 mm cassette under-samples large particles (>20 μm), relative to the human head (Kenny et al. 1997; Kenny et al. 1999). Compared with the 37 mm cassette, the IOM and Button samplers have sampling efficiencies that better match the IPM criterion (Mark and Vincent 1986; Grinshpun et al. 1995; Kalatoor et al. 1995). All of these size-selective samplers are limited; they do not report size distributions, only mass concentrations. Instruments capable of reporting the size distribution of aerosols exist, such as the Aerodynamic Particle Sizer (APS), Scanning Mobility Particle Sizer (SMPS) and various cascade impactors; however, these instruments are limited to particle sizes less than about 20 μm in aerodynamic diameter.

The APS reports concentration and size distribution for airborne particles from 0.5 to 20 μm and has been extensively used in laboratory and field studies (Chen et al. 1985; Baron 1986; Marshall et al. 1991; Armendariz and Leith 2002; Peters et al. 2006; Görner et al. 2010). Although extremely useful, the APS provides size distribution information for only a fraction of the inhalable range. At approximately 10 μm, the APS begins to experience issues with particle transmission efficiency into the detector (Volckens and Peters 2005).

Received 23 February 2015; accepted 9 August 2015.
Address correspondence to J. Volckens, Department of Mechanical Engineering, Colorado State University, 1374 Campus Delivery, Fort Collins, CO 80523, USA. E-mail: john.volckens@colostate.edu
Color versions of one or more of the figures in the article can be found online at www.tandfonline.com/uast.

Gibson, Vincent, and Mark (Gibson et al. 1987) developed the personal inhalable-dust spectrometer (PIDS), an eight-stage, cascade impactor with an entry designed to match the IPM criterion. The PIDS has been used to characterize the size distribution of aerosol particles in coalmines, bakeries, and primary lead smelters, where most of the mass is coarse. Mass median diameters of 41.6, 60.7, 67.3, and 71.4 μm were found in ore storage and milling, sinter pants, blast furnace, and drossing areas, respectively (Spear et al. 1998). Bimodal distributions were found in an automated bakery, egg powdery, cement factory, steel mill, spice factory, and in furniture carpentry, with large mass median diameters for the coarser mode ranging from 14 to 59 μm (Lidén et al. 2000). These studies demonstrate the presence of coarse dust in workplaces, with mass median diameters often above 40 μm.

Although the measurement of inhalable particles is difficult, accurate knowledge of their concentration and size is necessary to assess exposure and dose. Substantial differences exist in deposition to the oral, nasal, pharyngeal, and laryngeal regions for particles between 10 and 50 μm (Cheng et al. 1999); thus, the health effects of these particles can be substantially different. Particle deposition in the tracheobronchial region could potentially cause health effects such as asthma and bronchogenic cancer. Particles depositing in the oronasal cavities could result in health effects centered primarily in the upper respiratory region.

A high prevalence of occupational illnesses is related to inhalable-particle exposures. For example, occupational rhinitis occurs three times more frequently in occupational settings than occupational asthma (Bush et al. 1998). Exposure to animal dander (Slovak and Hill 1981; Kup 1985), flours (Moscato et al. 2008), wood dust (Kanerva and Vaheri 1993; Moscato et al. 2008), textile dust (Slavin 2003), food, spices, organic dusts, latex, and chemicals have all been associated with occupational rhinitis, as has exposure to pesticides (Slager et al. 2009). Furriers, spice workers, vegetable pickers, hemp workers, and grain handlers all have increased prevalence rates for self-reported sinusitis (El Karim et al. 1986; Zuskin et al. 1988a,b, 1990, 1993).

Sinonasal tumors are rare, but of all cancers have the second highest fraction attributable to occupational exposures (Rushton et al. 2012; Youlden et al. 2013). Exposure to wood dust (Andersen et al. 1977; Kleinsasser and Schroeder 1988; WHO 1995; Pesch et al. 2008), leather dust (Bonneterre et al. 2007), nickel compounds, radium-226, radium-228 and their decay products, and acids used in isopropyl alcohol production are all known risk factors for sinonasal cancer (Baan et al. 2009; El Ghissassi et al. 2009; Straif et al. 2009). Textile dust (Luce et al. 1997) and hexavalent chromium are possible risk factors for sinonasal tumors as well, but evidence is limited.

Retrospective epidemiological studies, exposure assessments, and the design of industrial hygiene controls are all hindered by this inability to monitor inhalable particles accurately. The objective of this study, therefore, was to develop a particle separator capable of characterizing concentrations and size distributions of inhalable-aerosol particles from 30 to 100 μm in aerodynamic diameter. The designs described here focus on sampling in calm air environments, as mean indoor wind speeds are generally less than 0.3 m s^{-1} in most workplaces (Baldwin and Maynard 1998).

DESIGN CONCEPT FOR THE PORTABLE INHALABLE-PARTICLE SEPARATOR (PIPS)

A schematic of the PIPS sampler is shown in Figure 1. The PIPS is based on the principles of a vertical elutriator. In the Stokes drag region, the terminal settling velocity of a particle, V_{TS}, occurs when the upward drag on a particle equals the downward force of gravity,

$$V_{TS} = \frac{d_p^2 \rho_p C_c g}{18\mu}, \qquad [2]$$

where d_p is particle diameter, ρ_p is particle density, C_c is the slip correction factor, g is the acceleration due to gravity, and μ is fluid viscosity (Hinds 1999).

For particle settling outside the Stokes region, where particle Reynolds number (Re_p) is greater than unity, Equation (2) loses accuracy. Instead, an alternative equation accurate within

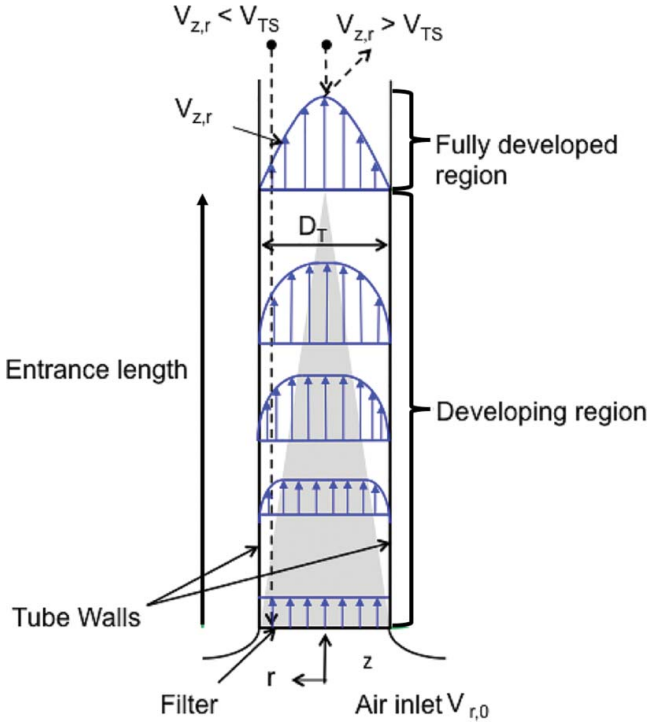

FIG. 1. Velocity profile in PIPS collection tube. The shaded triangular region depicts the width of the inviscid core region for a developing laminar flow.

3% for $1 < Re_p < 600$, can be used (Hinds 1999),

$$V_{TS} = \left(\frac{\mu}{\rho_g d_p}\right)\exp\left(-3.070 + 0.9935J - 0.0178J^2\right) \quad [3]$$

where

$$J = \ln\left(\frac{4\rho_p \rho_g d_p^3 g}{3\mu^3}\right) \quad [4]$$

and ρ_g is the gas density. For spherical particles settling in air at normal conditions, non-Stokes settling occurs for particles larger than approximately 80 μm in aerodynamic diameter.

The PIPS sampler operates by directing filtered air upward (vertically) through an open collection tube, in the opposite direction to a settling particle. If the upward air velocity in the tube is less than the particle's terminal settling velocity, then the particle should penetrate down through the tube and deposit on a filter at the bottom of the collection tube. If the upward air velocity is higher than the particle's terminal settling velocity, then the particle should be blown upward and out of the tube. Thus, the upward velocity can be varied in the PIPS collection tube to select a minimum particle size that will penetrate to the detection region. In this work, collection tube velocities were chosen to equal the terminal settling velocity of particles with aerodynamic diameters of 30, 40, 50, 60, 70, and 80 μm.

Ideally, the PIPS sampler would provide a sharp cut; that is, no particles smaller than the cut size, for which the particle's terminal settling velocity equals the upward air velocity in the collection tube, would be collected at all. Furthermore, all particles larger than the cut size would be collected completely. In this case, the cutoff curve, a plot of PIPS collection efficiency against particle diameter, would increase from zero to unity at the particle cut size.

Air Flow in PIPS Collection Tube

At the base of the PIPS, where the filter is located at the bottom of the collection tube, air exiting the filter is assumed to have a uniform upward velocity, V_0. As air flows upward through the tube, its velocity along the walls is reduced by friction. As the air velocity within this viscous boundary layer is reduced, conservation of momentum increases the velocity within the inviscid core (i.e., the centerline flow outside the boundary layer); for laminar flow, these phenomena produce a parabolic velocity profile (Figure 1). For fully developed laminar flow in a tube, the average velocity is approximately half of the velocity at the centerline. This parabolic profile will cease changing shape after a certain length, known as the entrance length, L_e, given by (Fargie and Martin 1971):

$$L_e \approx 0.06\, D_T\, Re_f, \quad [5]$$

where Re_f is the fluid Reynolds number and D_T is the diameter of the tube. Beyond L_e the inviscid core disappears and the fully developed flow maintains the same parabolic shape downstream.

The fluid flow inside the PIPS collection tube presents several challenges in the prediction of particle trajectories and collection. First, a nonuniform velocity profile at the top of the collection tube and beyond may affect particle trajectory toward the tube. Second, once particles are in the tube, the developing flow profile and corresponding velocity magnitudes, which change as a function of depth, may affect particle collection. Thus, particles that penetrate past the inlet of the sampler still may not reach the detection zone (in this case, a filter located at the base of the PIPS). If air at the top of the collection tube has a parabolic velocity profile, then a particle with aerodynamic diameter equal to the cut size that falls towards the tube could enter the tube or be blown out, depending on its initial radial position (Figure 1). Consider a 50 μm particle and a PIPS sampler operating at a cut size of 50 μm. If the particle falls relatively close to the tube wall and in the region where $V_{z,r} < V_{TS}$, then the particle will enter the collection tube. If the 50 μm particle falls close to the centerline and in the region where $V_{z,r} > V_{TS}$, then the particle will be ejected from the collection tube. As a result, the PIPS would not have the desired, sharp cut at 50 μm as some particles smaller than the cut size could enter but some particles larger than the cut size could be ejected.

The axial velocity profile within the collection tube also changes as particles approach the filter at the collection tube bottom. Particles smaller than the cut size that enter near the wall will encounter air with higher upward velocity as they approach the filter. Thus, the tendency for a velocity profile to allow particles smaller than the cut size to enter the collection tube near its wall is self-correcting, as these particles should not reach the filter (where velocity, V_0, is uniform across the filter face). On the other hand, particles larger than the cut size that fall near the tube centerline will be ejected and will not be sampled. PIPS collection should be low, as intended, for particles smaller than the cut size, but incomplete for particles larger than the cut size. A more pronounced velocity profile should cause a more gradual increase in collection efficiency with size.

The entrance length, L_e, at the top of the PIPS collection tube was calculated for each cut point from Equation (5). The percent of developed flow at the top of the collection tube was calculated by taking the ratio of the tube length to the entrance length (Table 1). Because the collection tubes used here were only a small fraction of L_e, the effect of velocity profile on particle sampling should be small.

TABLE 1
PIPS cut sizes (aerodynamic particle diameter) and associated filter velocity and flow properties

Particle cut size, μm	PIPS filter velocity, m s^{-1}	Entrance length, m	% Developed flow
30	0.027	0.111	13
40	0.048	0.197	7.6
50	0.075	0.307	4.9
60	0.108	0.440	3.6
70	0.148	0.570	2.6
80	0.193	0.709	2.1

ANALYTICAL FLOW SOLUTION AND SAMPLING EFFICIENCY

The Reynolds numbers associated with air flow through the PIPS collection tube are very low, from 60 to 370 for particle cut sizes from 30 to 80 μm, so that the air flowing out from the collection tube forms a dissipated laminar jet (Reynolds 1962; McNaughton and Sinclair 1966). Under these conditions the jet projects without mixing a certain distance into the still air, then disperses laterally. Analytical methods to describe jet flow at these low Reynolds numbers are not available. Although jet flow does not become fully turbulent until Reynolds number exceeds about 3000, equations for the propagation of a turbulent jet (Schlichting et al. 2000) were used here with the understanding that, at best, they give a rough approximation to actual flow conditions.

As a turbulent air jet enters quiescent air, a velocity shear is created between the jet and the air causing turbulence and mixing. The jet gradually expands, its upward velocity decreases (Figure 2), and it entrains some surrounding air. The radius of the jet is proportional to the distance downstream from the discharge location (Schlichting et al. 2000).

Calculated Velocity Profile

Schlichting's boundary theory (Schlichting et al. 2000) defines the characteristics of turbulent jets. The axial velocity profile is described by

$$\frac{V_{z,r}}{V_{\max}} = e^{-94(r/z)^2} \quad [6]$$

and the centerline velocity by

$$V_{\max} = 12\frac{D_T}{2z}V_o. \quad [7]$$

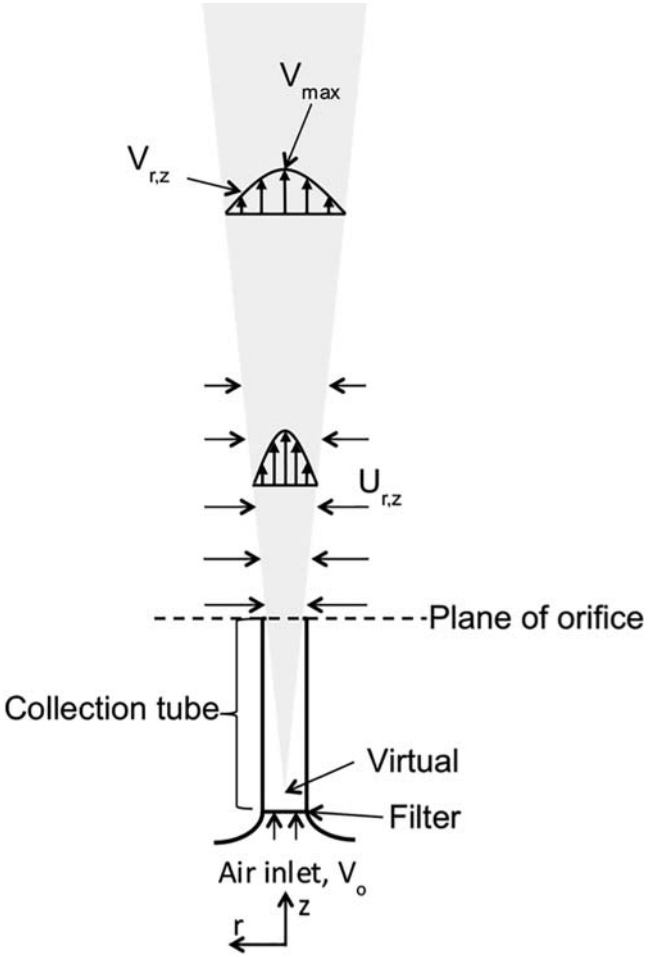

FIG. 2. Diagram of a turbulent jet exiting the PIPS. The shaded region represents the spreading jet. The virtual source is located inside the tube geometry and is the point from which the jet originates.

Combining Eqs. (6) and (7) gives

$$V_{z,r} = 12\frac{D_T}{2z}V_o e^{-94(r/z)^2}. \quad [8]$$

which allows the axial velocity profile to be solved as a function of axial distance from the jet origin, z, and radial distance from the jet centerline, r.

The initial radius of the jet that comes from the top of the collection tube is the radius of the tube. The equations of turbulent jet spreading are solved from a single point for the jet origin, called the virtual origin, located inside the tube where $z = 0$, and set as the axial distance where the axial velocity at the edge of the tube is half that at the centerline (Schlichting et al. 2000).

Radial air velocity was calculated using (Bird et al. 2007)

$$U_{z,r} = \frac{\left(\frac{Cv^*}{z}\right)\left(\frac{Cr}{z}\right) - 0.25\left(\left(\frac{Cr}{z}\right)^3\right)}{\left(1 + 0.25\left(C\frac{r}{z}\right)^2\right)^2}, \quad [9]$$

where C is a dimensionless integration constant (15.1), v^* is the turbulent kinematic viscosity given by (Bird et al. 2007).

$$v^* = \frac{\left(\frac{3}{16}\right)^{0.5} V_o \frac{D_T}{2}}{C}. \quad [10]$$

Axial and radial air velocities were solved for turbulent jets for the upward PIPS flow velocities defined in Table 1.

Calculated Particle Trajectories

Particle trajectories approaching the PIPS were calculated using the particle terminal settling velocity (Equations (3) and (4)) and jet velocities (Equations (8)–(10)). The initial particle release height was 100 cm above the jet at specified radial positions. The upward and radial velocities for the jet at the initial release position were calculated. The particle's axial velocity was estimated as a function of time and location by subtracting the axial jet velocity from the particle's terminal settling velocity. The particle's axial velocity times a nominal time step (0.05 s) was then subtracted from the initial axial position to compute the new axial position. The particle radial position was then updated using the initial radial distance plus the outward radial velocity times the time step. The particle's axial and radial positions were calculated until the particle's axial position was below the top of the PIPS collection tube. At that axial position, the particle's radial position was compared to the location of the tube wall. The initial radial particle release position was varied until the particle's final radial position was just inside the tube wall. PIPS efficiency was then calculated using

$$E = \left(\frac{x_p}{\frac{D_T}{2}}\right)^2. \quad [11]$$

where x_p is the initial radial particle release location and $D_T/2$ is the radius of the collection tube.

DESIGN CONCEPT FOR JET-FREE PIPS (PIPSv2)

As discussed above, jet effects at the air outlet (particle inlet) at the top of the PIPS collection tube could affect particle sampling efficiency. To reduce any such problems a second sampler design, the PIPSv2, was developed to create a stagnation point directly above the inlet of the upward-facing collection tube.

Figure 3 is a diagram of the PIPSv2 sampler with relevant dimensions. As in the PIPS design, clean air flows upward through a filter and into a collection tube. However, the PIPSv2 sampler has a cap with a round inlet opening that is centered directly above the collection tube. Below this cap, air coming from the collection tube is pulled radially outward into an annular space between the cap and tube walls, and from there out the bottom of the sampler. This exhaust flow is set to equal the upward flow through the collection tube so that no air enters the sampler through the cap inlet opening. Table 2 gives the flow rates for the PIPSv2 sampler. As the upward flow from the collection tube bends radially outward, it forms an axial stagnation point below the cap inlet. From this stagnation point, smaller particles that fall through the cap inlet opening are carried away with the radial, outward flow, whereas larger particles fall into the collection tube. This

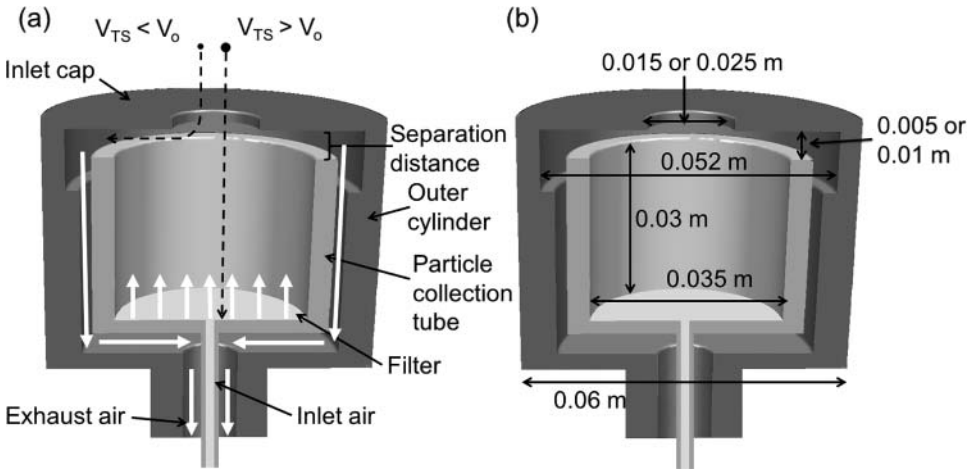

FIG. 3. PIPSv2 design schematic illustrating (a) airflow and particle behavior and (b) dimensions. White arrows indicate airflow direction; dashed lines indicate potential path lines for particles entering the sampler.

TABLE 2
PIPSv2 flow rates for each cut size

Particle cut size, μm	Flow rate, L min^{-1}
30	1.31
40	2.34
50	3.64
60	5.21
70	6.76
80	8.40

TABLE 3
CFD simulation variables

Sampler	Inlet opening, m	Separation distance, m	Cut sizes, μm
PIPS	0.032	NA	30, 40, 50, 60, 70, 80
PIPSv2	0.015	0.005	30, 40, 50, 60, 70, 80
		0.010	
	0.020	0.005	30, 40, 50, 60, 70, 80
		0.010	
	0.035	0.005	50
		0.010	

design eliminates the jet that emanates from the top of the collection tube and should improve the sharpness of the resultant cutoff curve.

Separation distance, defined as the gap between the bottom of the inlet cap and the top of the collection tube, was varied to determine its effect on the cutoff curve. Two separation distances were investigated: 5 and 10 mm. The diameter of the inlet opening in the PIPSv2 cap was varied as well (15, 20, and 35 mm).

COMPUTATIONAL FLUID DYNAMICS (CFD) MODELING OF PIPS AND PIPSv2

CFD modeling was conducted to investigate airflow, particle transport, and sampling efficiencies for the PIPS and PIPSv2 operating in calm air. Ansys software (Design Modeler, Meshing application, and Fluent 14.0, Ansys Lebanon, NH, USA) was used to create the geometry, generate the mesh, and solve the equations of fluid flow. Steady-state, incompressible Navier-Stokes equations were used to model flow. Once the fluid flows were solved and the quality of the solution assessed, laminar particle trajectories were simulated to determine sampler efficiency. Six cut sizes were investigated: 30, 40, 50, 60, 70, and 80 μm (Table 1). CFD modeling details are included in the online supplementary information. The PIPS sampler was modeled as a tube with an inner diameter of 0.032 m, an outer diameter of 0.037 and 0.015 m high. The PIPSv2 sampler was modeled as an interior collection tube with an inner diameter of 0.035 m, an outer diameter of 0.037 m and 0.030 m high. The cap had an inside diameter of 0.052 m and outer diameter of 0.060 m. Six sampler geometries were investigated for PIPSv2: three cap inlet openings and two separation distances (Table 3). The effect of sampler geometry on efficiency was investigated for the 50 μm cut size. Both PIPS and PIPSv2 were modeled 0.254 m above the floor in the center of a calm-air chamber with dimensions of 1 m × 1 m × 1 m. Simulated sampler efficiency was calculated by taking the ratio of the upstream area where particles were aspirated to the cross-sectional area of the collection tube and filter, analogous to Equation (11).

Sampler Fabrication and Design

The PIPS sampler (Figure 4a) utilized a vertical collection tube 32 mm inner diameter (ID) and 15 mm in length, with its base fitted into a 37 mm filter cassette. A short tube length was selected so that the effects of nonuniform axial velocities on particle sampling efficiency (i.e., a parabolic laminar flow profile) were minimized within the tube. The PIPS collection tube was made from aluminum to minimize electrostatic effects. An O-ring was situated at the base of the collection tube to provide sealing between the tube and the filter cassette. A coarse filter (Cellulose Support Pad, Pall) was chosen because of its rigidity under positive pressure (via upward airflow). A rubber plug with a hose-barb fitting was placed over the top of the collection tube to calibrate airflow through the PIPS.

The PIPSv2 sampler (Figures 4b–d) had a vertical collection tube 30 mm long with an inner diameter (ID) of 35 mm and an outer diameter (OD) of 37 mm, which also allowed a 37 mm filter and cassette to be attached to its bottom. Cap openings of 15 and 20 mm, and separation distances between the bottom of the cap and the top of the collection tube of 5 and 10 mm, were investigated to inform the optimal settings for a sharp cutoff (Figure 4c). The outer tube had ID and OD of 40 and 42 mm, respectively. The PIPSv2 was made from aluminum for durability and to minimize electrostatic effects, and weighed approximately 750 g. Two rotary vane pumps (GAST rotary vane oil vacuum pump, model 0323) provided the necessary airflows (Table 2); each was controlled by a separate needle valve. Calibrated rotameters monitored flows during a given test and were adjusted as necessary to ensure balanced flow. If the flow varied more than 10% over the test, then the test was considered invalid and repeated.

Test Chamber

A vertical, calm-air chamber (2.5 m high with 1 m × 1 m cross-section) was used to investigate the collection efficiency of the samplers (Figure 5). The aerosol dispersion system,

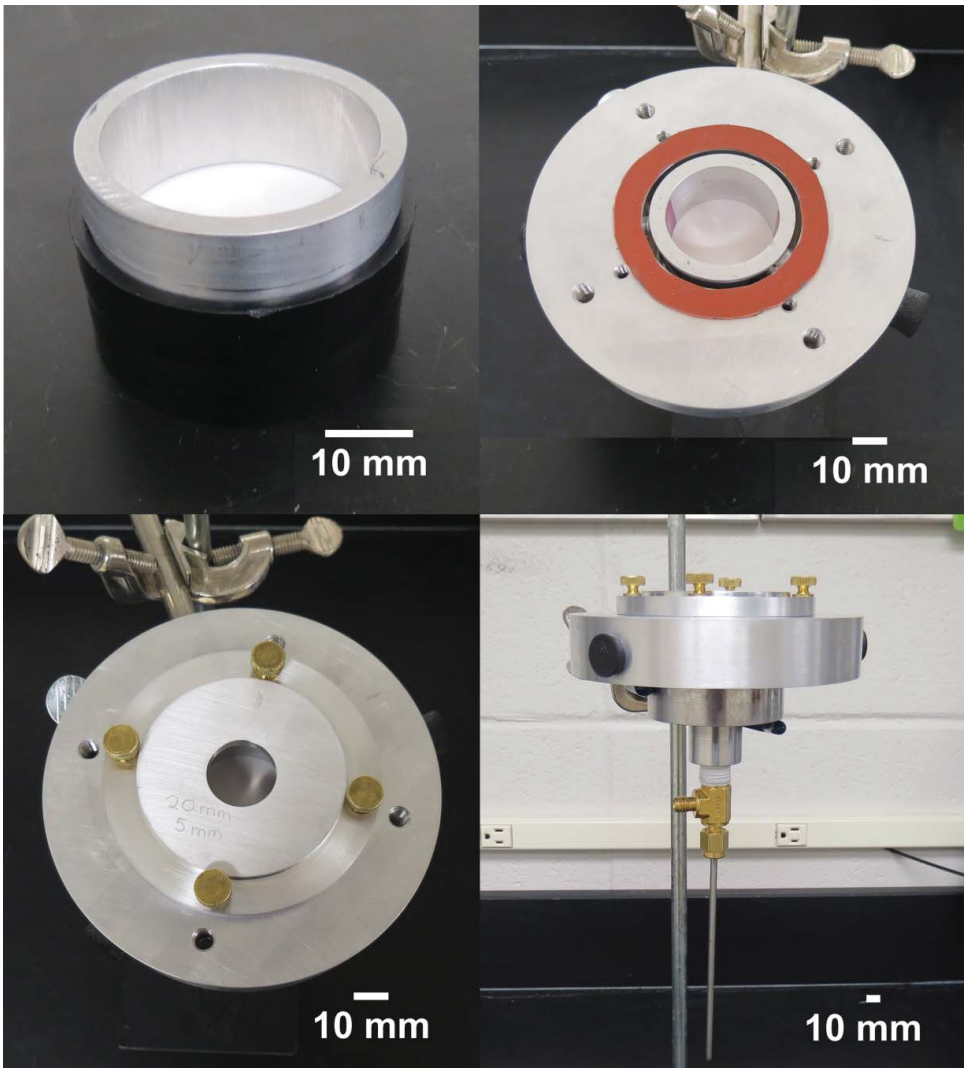

FIG. 4. (a) PIPS sampler, (b) top view of the opened PIPSv2 sampler, (c) PIPSv2 seen from above with inlet cap, and (d) side view of the PIPSv2 sampler. The annular slit in (b) carries the upward flow away from the inlet, forming a stagnation point and the center of the PIPSv2 inlet in (c).

located in the upper section of the chamber, was comprised of a cap holding 0.1 g of test powder connected to a compressed nitrogen source. A solenoid valve was attached to the compressed nitrogen line. When the valve was opened, a jet of nitrogen ejected the test powder into the chamber. The nitrogen jet was activated once, for fewer than 5 s, to aerosolize the test particles. A honeycomb diffusor (25 mm cell size) was located in the center of the chamber (at a height of 1.25 m) to break up any turbulent eddies generated during powder dispersion (keeping the lower half of the chamber relatively quiescent). The aerosol was then allowed to settle for 10 min, sufficient for the smallest particles of interest to reach the base of the chamber.

Three reference samplers and either the PIPS or PIPSv2 were located in a square pattern centered in the middle of the chamber floor. The reference samplers were open, 37 mm cassettes holding filters like the one used in the PIPS or PIPSv2 sampler. They were located 250 mm above the chamber floor, above the inlet of the PIPS or PIPSv2 sampler, to minimize the influence of jet effects or particles ejected from the PIPS or PIPSv2 sampler during measurements. After each powder injection, the filters in the reference and test samplers were changed, and the PIPS or PIPSv2 rotated to a different corner of the square. This process was repeated until four tests were made, one with the PIPS or PIPSv2 in each corner of the square pattern. This set of four tests comprised one experiment.

The polydisperse test powder was fluorescent, polyethylene microspheres of unit density with sizes ranging from 10 to 90 μm (UVYGPMS, Cospheric LLC). An epifluorescent microscope (Orthoplan, Leica) and fluorescence filters (Vivid Plus Set XF05–2/B, Omega Optical) were used to

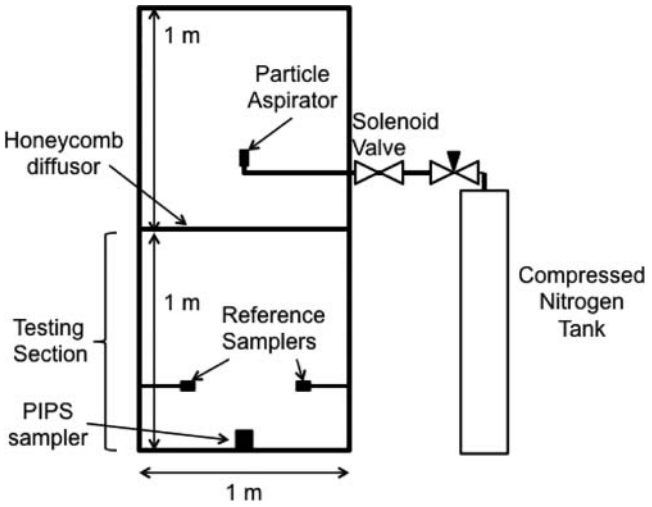

FIG. 5. Schematic of the calm-air chamber and experimental setup. Particles are aspirated into the upper section of the calm-air chamber and settle into the testing section. Reference samplers are located in the testing section.

image collected particles. Filters were imaged under a 1.6x objective lens and a 10x objective eyepiece. ImageJ software (NIH, V1.46r [Rasband]) was used to obtain the area of each particle, from which the corresponding particle aerodynamic diameters were calculated using Microsoft Excel. A stage micrometer provided a reference for ImageJ size analysis. Size distributions of the reference samplers were measured using microscopic analysis following the procedure outlined above. Particles were sorted by aerodynamic diameter into one of nine size bins from 15 to 95 μm, each with a 10 μm bin width. Figure 6 shows particles from a reference sampler photographed and analyzed using this procedure.

Deposition patterns in the chamber were assessed to ensure that particles were dispersed uniformly. The test aerosol was dispersed into the chamber, and size and count statistics generated at the four sampling locations.

Measurement of Sampling Efficiency

Three replicate experiments of four tests each were conducted for six particle size cuts (30, 40, 50, 60, 70, and 80 μm) for a total of 18 experiments per sampler. Fractional sampling efficiency (η_j) was computed for each size cut,

$$\eta_j = \frac{N_{s,j}}{N_{R,j}} \quad [12]$$

where $N_{s,j}$ is the number of particles observed on the sampler filter for the jth size range and $N_{R,j}$ is the average number of particles observed on the three reference filters for the jth size.

Velocity Measurements

Velocity measurements for the 70 μm cut were taken above the PIPS collection tube to compare experimental jet velocities to those estimated by the analytical and CFD models. Jet velocity was measured using a thermal anemometer (AVM440, TSI, Shoreview, MN, USA) directly above the center of the PIPS inlet and at distances of 10, 20, 40, and 100 mm above this location. Measurements were also taken radially from the flow axis centerline at ±10 and ±15 mm. Measurements were taken for 10 s and then averaged. This process was repeated five times at each location. Measured velocities were plotted and compared to the simulated laminar and analytical turbulent velocity profile.

Data Analysis

The spatial uniformity of test aerosol dispersed within the test chamber was assessed using ANOVA to compare the size distributions at each reference sampling location. Tukey's method of multiple comparisons was used to determine whether any locations were significantly different.

A general linear mixed model was used to compare cutoff curves of the PIPS and PIPSv2 samplers. Tests of the slopes were conducted to determine if the PIPSv2 sampler had

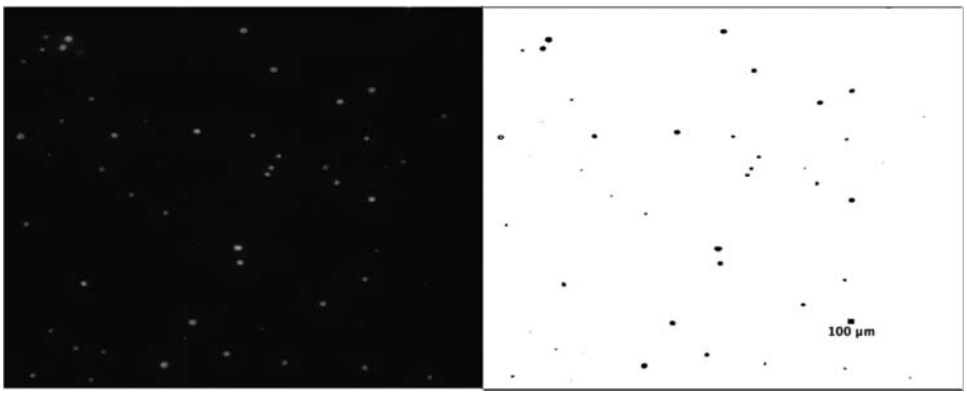

FIG. 6. Image of particles on a reference filter. On the left is the raw fluorescent image and on the right is the ImageJ rendering.

significantly sharper cuts. Percentage difference between experimental sampling efficiency and simulated sampling efficiency was calculated for each cut point. An ANOVA was used to determine whether cap inlet diameter and separation distance had a meaningful influence on the slope of the sampling efficiency curves of the PIPSv2 sampler.

Sampling efficiency curves for the PIPS and PIPSv2 samplers were well represented by logistic functions:

$$\hat{\eta}_j = D + \frac{(A-D)}{1+\left(\frac{d_j}{C}\right)^B} \quad [13]$$

where $\hat{\eta}_j$ is the modeled sampling efficiency for a particle with aerodynamic size j, and the coefficients A, B, C, and D were obtained by nonlinear, least-squares regression (SAS, v9.4). Tables 4 and 5 lists coefficient values at all cut sizes for both the PIPS and PIPSv2 samplers.

Data Inversion Procedure to Obtain Size Distribution

To determine how effectively the PIPS and PIPSv2 samplers could measure the size distribution of a coarse aerosol, additional experiments were conducted with both samplers operated at each of its six cut sizes. For these experiments, only the total number of particles collected on the PIPS or PIPSv2 filter at each cut size was measured. These data were then used to estimate the number concentration and size distribution of the test aerosol as described below, then compared with data collected simultaneously using the reference samplers.

Data inversion techniques can be used to estimate a continuous size distribution from measured particle counts in discrete bins. The simplest approach is to assume a perfectly sharp cut, then to fit a curve through a plot of the cumulative counts deposited in successive stages as a function of particle aerodynamic diameter. Typically, prior assumptions are made that the aerosol is log-normally distributed; however, many distribution curves can be fitted to the discrete data points. The sampling efficiency curves for PIPS were not sharp so that this simplistic approach was not appropriate; as a result, the following data inversion procedure was used.

TABLE 4
Experimental coefficients for Equation (4) for the PIPS sampler and each cut point PIPS Sampler

	Coefficient			
Particle aerodynamic cut size, μm	A	B	C	D
30	5.0e-2	6.2	36	1.2
40	0.00	6.8	49	1.0
50	0.00	5.5	73	1.3
60	1.0e-2	10.3	71	0.95
70	3.0e-2	14	79	0.85
80	2.0e-2	16	77	0.61

TABLE 5
Experimental coefficients for Equation (4) for the PIPSv2 sampler and each cut point PIPSv2 Sampler

	Coefficient			
Particle aerodynamic cut size, μm	A	B	C	D
30	0.00	53	25	1.0
40	1.0e-2	11	48	0.86
50	4.0e-2	13	54	1.1
60	1.0e-2	13	62	0.98
70	0.00	14	71	0.82
80	2.0e-2	23	74	0.67

A logistic function was fitted to the sampling efficiency curves for each cut point. The coefficients were obtained by nonlinear, least-squares regression. Next, an initial approximation of a count median diameter (CMD) of 52 μm and standard deviation (SD) of 15 μm were used as a random starting point; these CMD and SD values were then adjusted through a series of iterations to arrive at the optimal solution. A data-inversion spreadsheet was developed in Microsoft Excel (2010, Microsoft Corp., Seattle, WA, USA) to estimate the CMD, SD, and number concentration of a normally distributed, unimodal aerosol from particle number concentrations measured with the PIPS sampler at six cut points following the method described by O'Shaughnessy and Raabe (O'Shaughnessy and Raabe 2003). An initial guess for the number concentration was taken as the number concentration for the 30 μm cut.

RESULTS

Jet Velocities

For the PIPS sampler, the laminar jet profile from the CFD simulations was compared to the turbulent jet from the analytical solutions for the 70 μm cut. The centerline velocity decayed more rapidly for the turbulent analytical model compared to the simulated laminar jet. These trends compared well to published experimental observations (Labus and Symons 1972). Measured velocities decayed more rapidly at lateral distances from the PIPS centerline. At increased vertical distances from the PIPS sampler, velocity decayed more rapidly than predicted by laminar jet theory.

Inspection of the CFD velocity vectors and flow streamlines showed the PIPSv2 had a flatter velocity profile than the PIPS sampler throughout its collection tube. As intended, small particles were pulled radially outward, and large particles fell into the PIPSv2 collection tube.

Spatial Uniformity of Particles in the Calm-Air Chamber

Particle deposition in the test chamber was relatively uniform across the four quadrants on the chamber floor (Table 6). Location C had slightly higher particle counts than the other locations; however, variations in the size distributions between the locations were not significantly different ($p = 0.23$).

PIPS Sampling Efficiency

The experimental and simulated sampling efficiency curves at the six cut points for the PIPS and PIPSv2 samplers are displayed in Figure 7. The error bars in this figure represent one standard deviation based on the variability between sampling efficiency measurements for repeated experiments. The experimental PIPS sampler efficiency showed good agreement with the CFD model and the theoretical solution. As particle size increased, the measured PIPS sampler efficiency deviated more from the simulated sampling efficiency: the cut point became less sharp, and measured sampling efficiency for particles larger than the cut size was less than 100%. Experimental sampling efficiency was substantially higher than the simulated sampling efficiency for the 80 μm cut.

Although the PIPS sampler was predicted to perform reasonably well, particle separation curves were not as sharp as desired (Figure 7). Analytical solutions and CFD simulations both predicted sampling efficiencies less than 100% for particles above the cut size for all cut sizes investigated. The analytical solutions predicted slightly lower sampling efficiencies than the CFD simulations, with the differences most apparent for particle sizes near the cut point. Analytical and CFD determined efficiencies deviated most for the largest cut size, 80 μm.

Airflow in the PIPS tube that was more developed than predicted by the analytical equations could account for some lack of sharpness in the sampling efficiency curves. Velocity vectors and flow streamlines in the CFD simulations showed centerline velocities 10% higher than appropriate for the desired cut point, despite the use of a collection tube just 15 mm long.

Wall losses inside the PIPS collection tube were evaluated using CFD modeling and found to be minimal. Fewer than 5% of the incoming particles deposited on the walls for all cut sizes. Thus, wall deposition should not substantially affect sampling efficiency.

TABLE 6
Aerodynamic particle size and count statistics for locations in the calm-air chamber

Location	Count median diameter, μm (std. dev.)	Number of particles (std. dev.)
A	54.9 (30.2)	182 (22)
B	63.2 (29.2)	248 (63)
C	58.2 (30.0)	313 (64)
D	62.9 (29.8)	246 (41)

PIPSv2 Sampling Efficiency

The PIPSv2 sampler was designed to minimize the jet effect at the top of the PIPSv2 collection tube while maintaining a flat velocity profile throughout the tube. Experimental sampling efficiency for the PIPSv2 sampler compared reasonably well to CFD simulations. The 70 and 80 μm cuts had the greatest differences between experimental and simulated efficiencies, with experiments underestimating simulated sampling efficiencies by 20%–30% for particles larger than the cut size. The PIPSv2 sampler had much higher sampling efficiencies and steeper cuts than the PIPS sampler, especially for the 50 and 60 μm cut points.

PIPSv2 inlet openings of 15 and 20 mm resulted in sharper efficiency curves with sampling efficiencies near 100% for particles just larger than the cut point (Figure 8). For inlet openings of 35 mm, sampling efficiency was not as sharp. For the 35 mm inlet opening, CFD particle trajectory simulations showed particles impacting on the lip of the collection tube. Separation distances of 5 and 10 mm, respectively, had little effect on the sampling efficiency, on average less than 1%. The 10 mm separation distance (for both the 15 and 20 mm inlets) resulted in slightly steeper cutoff curves and less small particle contamination. The 5 mm separation distance was less effective at preventing small particles from reaching the detection region.

Data Inversion to Obtain Size Distribution

Fluorescence microscopy of the reference sampler filters produced a CMD of 62 μm and a standard deviation of 20 μm (Figure 9). Inversion of the PIPS data resulted in a CMD of 72 μm and a standard deviation of 16.5 μm. The PIPSv2 data resulted in a CMD of 67 μm and a standard deviation of 19 μm. Both samplers characterized the CMD and standard deviation reasonably well, although the PIPS sampler somewhat overestimated the CMD.

DISCUSSION

The sampling efficiency of the PIPSv2 sampler was better than that of the PIPS sampler. The separation efficiency curves were sharper and overall sampling efficiency higher for the PIPSv2 sampler. With PIPSv2, sampling efficiency for particles larger than the specified cut was nearly 100%, a substantial improvement over the PIPS sampler. Reasonable agreement exists between the analytical solution, CFD simulations, and experimental collection efficiencies of the PIPS sampler (Figure 7). The CFD simulations and analytical solutions tended to slightly underestimate sampling efficiency compared to the experimental tests; however,

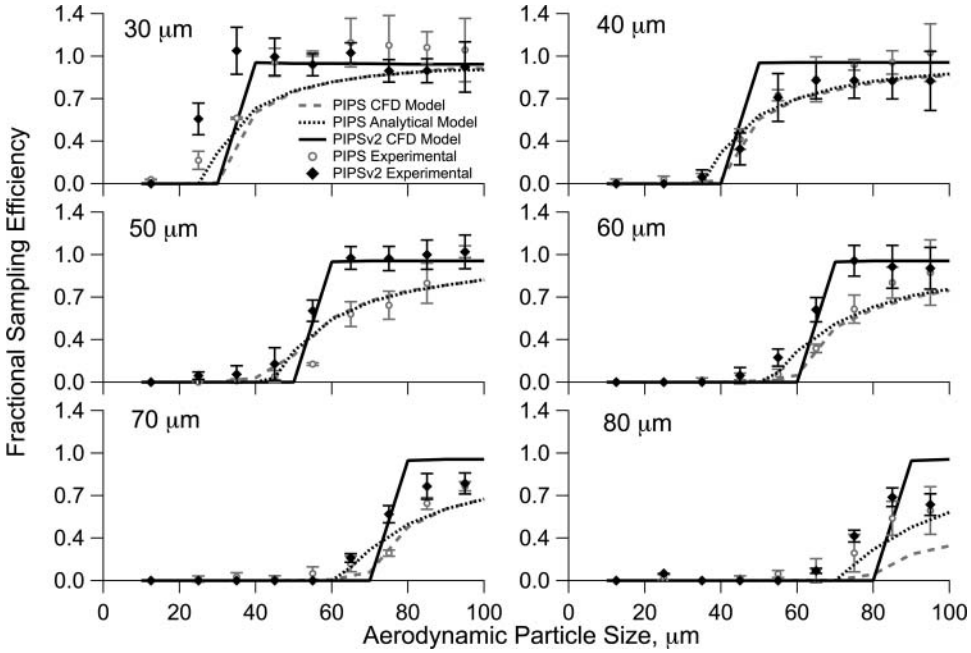

FIG. 7. Experimental and simulated sampling efficiency for the PIPS and PIPSv2 samplers for (a) 30, (b) 40, (c) 50, (d) 60, (e) 70, and (f) 80 μm cut points. CFD modeling of the PIPSv2 sampler (20 mm inlet, 5 mm separation distance) is represented by the solid line; CFD modeling of the PIPS sampler is represented by the dashed grey line. The experimental PIPSv2 results are represented by the solid markers and the experimental PIPS results are represented by the open markers.

differences in sampling efficiencies among the three methods were within 10%.

Inlet openings of 15 and 20 mm resulted in sharp cutoffs for the PIPSv2, while the inlet opening of 35 mm resulted in sampling efficiencies similar to those found for the PIPS design. Separation distance had minimal effect on sampling efficiencies. Separation distances may have been too large, which could have caused removal of large particles that should have deposited on the filter. Cascade impactor theory recommends minimum jet-to-plate distance (S) to jet width (W) ratios of 1. The 15 mm inlet with 10 mm separation resulted in a S/W ratio of 0.67, which of the design

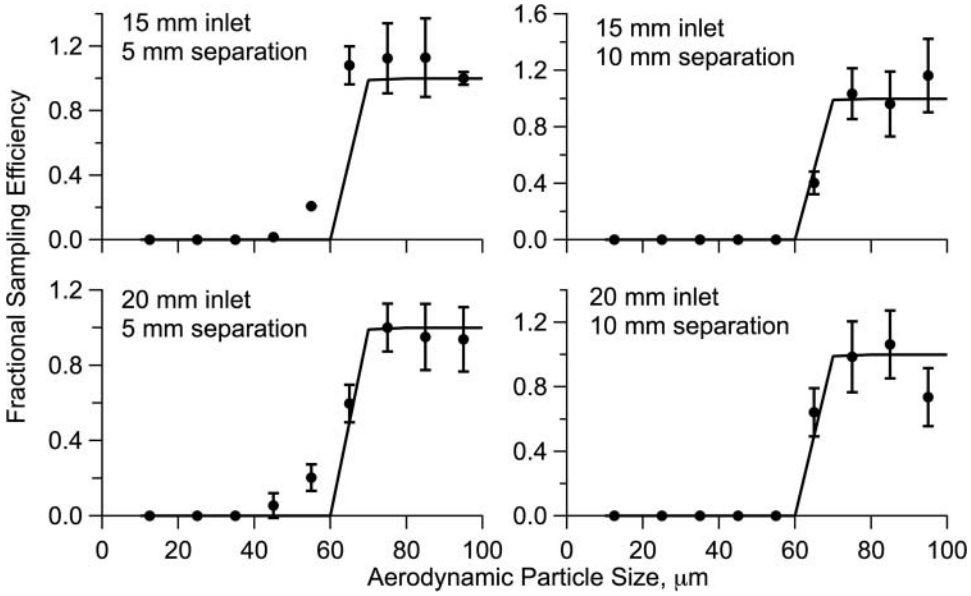

FIG. 8. Effect of inlet size and separation distance on PIPSv2 sampling efficiency. All tests shown for a 70 μm cut size. Error bars represent one standard deviation about repeated tests.

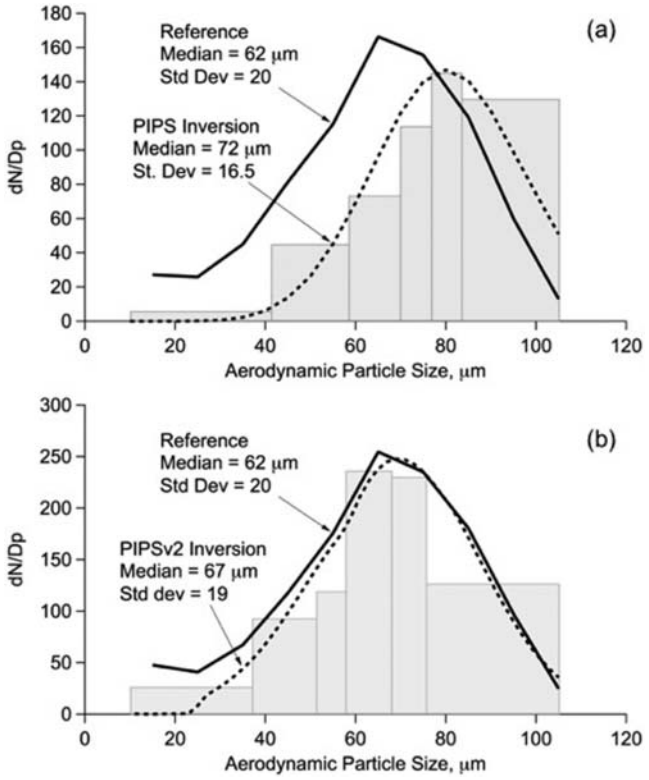

FIG. 9. Size distribution in the chamber estimated by (a) PIPS and (b) PIPSv2 samplers. The reference size distribution was measured by optical microscopy of settled dust (solid line in both graphs). The light-gray bars represent the raw particle counts for each stage.

parameters investigated in this study was closest to this recommended minimum. This fact could be why the 15 mm inlet and 10 mm separation resulted in the sharpest cutoff curves. Cascade impactor theory also recommends Reynolds numbers between 500 and 1000 for sharp cutoff curves. The Reynolds numbers for this study ranged from 27 to 256, well below the recommendation. Although the PIPSv2 design is quite different from that of a virtual impactor (air is not being accelerated toward an inner collection substrate), future work should take advantage of impactor theory to guide the next design iterations. Although the collection efficiencies were not as sharp or as high as desired, the PIPSv2 design did remove the presence of the jet at the top of the collection tube.

Although sampling efficiency is improved with the PIPSv2 sampler, flow control and sampler geometry are more complex. The PIPSv2 sampler relies on balanced airflow between the air flowing up and the air pulled out. If these flows are not well balanced, sampling efficiency could be adversely affected. Misalignment of the interior collection tube and the outer cup could create a flow imbalance across the top of the collection tube and affect the cutoff curves.

Upward flow from the PIPS collection tube was modeled as a turbulent jet for the analytical work, but laminar for the CFD work. Despite the differences in these models, the sampling efficiency curves showed good agreement. Although airflow within the PIPS collection tube compared well with theory for laminar flow, flow in the jet outside the tube was higher. The higher centerline velocity and radial spreading of the jet can help account for the gradual increase in sampling efficiency for the PIPS.

If particles smaller than the cut size enter the collection tube near its wall, they will be able to penetrate into the tube but will not reach the filter collection zone. These particles may hover in the tube until they either deposit on the wall or travel radially into the center region of higher velocity where they will subsequently be blown out. Particles with terminal settling velocities near the cut point will penetrate into the tube but then hover above the filter. As larger particles fall through the tube, they may impact the hovering particles and remove them from the airstream. Particles hovering above the filter may also agglomerate and then deposit on the filter. Both of these phenomena would result in particles smaller than the cut size penetrating to the filter collection zone. The air velocity along the edges of the PIPS collection tube is slower than along the centerline, due to viscous drag along the walls. If particles enter the collection tube near the walls (within the viscous boundary layer), particles smaller than the specified cut point may penetrate past the inlet and into the collection tube. As these particles descend, they eventually reach a point where the viscous boundary layer is not sufficiently developed; eventually the particle's terminal settling velocity is matched by the (developing) upward flow velocity. These particles theoretically "hover" in the collection tube until they either deposit on the wall, travel radially into a region of higher velocity where they are subsequently blown out, or the airflow is turned off and they fall to deposit on the filter. Furthermore, particles with terminal settling velocities slightly higher than that of cut point particles will enter the tube, but then fall slowly and tend to hover above the filter. Larger particles that fall through the tube may impact these hovering particles and carry them to the filter. Hovering particles may also impact each other to form agglomerates that then deposit on the filter. Images of the samplers were examined to determine if particle aggolmerations were occuring in the collection tube. The sampler filters had fewer agglomerates than the reference filters, indicating that particle agglomeration in the collection tube is rare. Particle deposition on the walls was not evaluated quantitatively; however, visual inspection of the sampler walls did not reveal substantial deposits on the walls (to note – the particles tested here were large enough to be visible by the naked eye when present on the surface of the exterior of the sampler).

This article describes PIPS and PIPSv2 instruments that employ a single collection tube that classifies a coarse aerosol into two fractions – one larger and one smaller than a specified cut size. To measure the size distribution of an aerosol, a PIPS or PIPSv2-based spectrometer could be constructed in one of two ways. One such spectrometer would employ multiple

collection tubes that operate simultaneously, each with a different cut size. Another such spectrometer would employ a single collection tube operated in a way that steps through a series of cut sizes by sequentially adjusting its air flow and changing the filter between cut sizes. This spectrometer would be appropriate when the aerosol to be characterized is stable over the time necessary to step through the required flows. Both spectrometers would benefit from a real-time particle sensor. Incorporating a photodiode/detector into the sampler for particle detection by light scattering could provide real-time analyses that would be useful for determining exposures in workplaces. Although most of the diseases associated with large particle exposure are chronic rather than acute, real-time measurements would be helpful to pinpoint where sources of exposure are occuring so that appropriate control actions can be taken. Work on this topic is in progress.

This work was designed as a proof-of-concept. Further investigation is necessary to determine the effect of particle projections, cross-winds, and the range of low velocity wind speeds on collection efficiency. For use in occupational settings, the appropriateness of the inlet efficiency should also be examined and compared to the inhalability fraction. Future work could also simplify the PIPSv2 design by using one pump, with suction from the annulus and pushing air out from the pump through the filter at the bottom of collection tube.

CONCLUSION

This article describes the development of two devices capable of size-selective sampling of inhalable particles. Ideally, both samplers would provide sharp cutoff curves. While the PIPS sampler is capable of size-selective sampling, its cutoff curves were not sharp. Compared to PIPS, the PIPSv2 sampler provided considerably sharper efficiency curves and higher sampling efficiencies for particles larger than the cut size.

These samplers could be beneficial to exposure assessment scientists and industrial hygienists. Until now, hazards associated with exposure to large, inhalable particles have not been quantified due to a lack of measurement technology. Development of real-time capabilities for these samplers would expand their usefulness, as large inhalable particles settle quickly through air; such efforts will be the subject of future work. The PIPS and PIPSv2 samplers could be used to determine size distribution of aerosols as a function of job task or to evaluate how aerosol size distribution changes over time. The samplers described in this article may allow practitioners to assess worker exposure more precisely, select better control methods, and improve our understanding of adverse health effects and target organs from exposure to large inhalable particles.

NOMENCLATURE

C_c	slip correction factor
C	dimensionless integration constant
CMD	count median diameter
d_{ae}	particle aerodynamic diameter
d_p	particle diameter
D_T	collection tube diameter
g	acceleration due to gravity
ID	inner diameter
IF	inhalable fraction
L_e	entrance length
$N_{s,j}$	number of particles observed on the sampler filter for the jth size range
$N_{s,j}$	average number of particles observed on the three reference filters for the jth size
OD	outer diameter
r	radial distance from the flow centerline
Re_f	fluid Reynolds number
Re_p	particle Reynolds number
SD	standard deviation
$U_{z,r}$	radial air velocity as a function of vertical distance from the virtual origin (z) and horizontal distance (r) from the flow centerline
V_{max}	maximum centerline velocity
v^*	turbulent kinematic viscosity
V_0	air velocity at the base of the PIPS immediately after the filter
V_{TS}	terminal settling velocity
$V_{z,r}$	axial air velocity as a function of vertical distance from the virtual origin (z) and horizontal distance (r) from the flow centerline
x_p	initial radial particle release position
z	axial distance from collection tube filter face ($z = 0$ at virtual origin)
μ	fluid viscosity
η_j	fractional sampling efficiency
ρ_g	gas density
ρ_p	particle density

ACKNOWLEDGMENTS

The authors would like to thank Christian L'Orange for helping design and manufacture the PIPS and PIPSv2 samplers. The contents are solely the responsibility of the authors and do not necessarily represent the official views of National Institute for Occupational Safety and Health (NIOSH).

FUNDING

This work was funded by the National Institute for Occupational Safety and Health (NIOSH), Center for Disease Control (R21OH010117).

SUPPLEMENTAL MATERIAL

Supplemental data for this article can be accessed on the publisher's website.

REFERENCES

Andersen, H., Andersen, I., and Solgaard, J. (1977). NASAL CANCERS, SYMPTOMS and Upper Airway Function in Woodworkers. *Br. J Ind. Med.*, 34:201–207.

Armendariz, A. J., and Leith, D. (2002). Concentration Measurement and Counting Efficiency for the Aerodynamic Particle Sizer 3320. *J. Aerosol Sci.*, 33:133–148.

Baan, R., Grosse, Y., Straif, K., Secretan, B., El Ghissassi, F., Bouvard, V., Benbrahim-Tallaa, L., Guha, N., Freeman, C., and Galichet, L. (2009). A Review of Human Carcinogens—Part F: Chemical Agents and Related Occupations. *Lancet Oncol.*, 10:1143–1144.

Baldwin, P. E., and Maynard, A. D. (1998). A Survey of Wind Speeds in Indoor Workplaces. *Ann. Occup. Hyg.*, 42:303–313.

Baron, P. A. (1986). Calibration and Use of the Aerodynamic Particle Sizer (APS 3300). *Aerosol Sci. Technol.*, 5:55–67.

Bird, R. B., Stewart, W. E., and Lightfoot, E. N. (2007). *Transport Phenomena*. John Wiley & Sons.

Bonneterre, V., Deschamps, E., Persoons, R., Bernardet, C., Liaudy, S., Maitre, A., and de Gaudemaris, R. (2007). Sino-Nasal Cancer and Exposure to Leather Dust. *Occup. Med.*, 57:438–443.

Bush, R. K., Wood, R. A., and Eggleston, P. A. (1998). Laboratory Animal Allergy. *J. Allergy Clin. Immunol.*, 102:99–112.

Chen, B., Cheng, Y., and Yeh, H. (1985). Performance of a TSI Aerodynamic Particle Sizer. *Aerosol Sci. Technol.*, 4:89–97.

Cheng, Y.-S., Zhou, Y., and Chen, B. T. (1999). Particle Deposition in a Cast of Human Oral Airways. *Aerosol Sci. Technol.*, 31:286–300.

El Ghissassi, F., Baan, R., Straif, K., Grosse, Y., Secretan, B., Bouvard, V., Benbrahim-Tallaa, L., Guha, N., Freeman, C., and Galichet, L. (2009). A Review of Human Carcinogens—Part D: Radiation. *Lancet Oncol.*, 10:751–752.

El Karim, M. A. A., El Rab, M. O. G., Omer, A. A. A., and El Haimi, Y. A. (1986). Respiratory and Allergic Disorders in Workers Exposed to Grain and Flour Dusts. *Arch. Environ. Health*, 41:297–301.

Eller, P. M., and Cassinelli, M. E. (1994). *NIOSH Manual of Analytical Methods*. DIANE Publishing.

Fargie, D., and Martin, B. (1971). Developing Laminar Flow in a Pipe of Circular Cross-Section. *Proceedings of the Royal Society of London A: Mathematical, Physical and Engineering Sciences*. 321:461–476.

Gibson, H., Vincent, J., and Mark, D. (1987). A Personal Inspirable Aerosol Spectrometer for Applications in Occupational Hygiene Research. *Ann. Occup. Hyg.*, 31:463–479.

Görner, P., Simon, X., Wrobel, R., Kauffer, E., and Witschger, O. (2010). Laboratory Study of Selected Personal Inhalable Aerosol Samplers. *Ann. Occup. Hyg.*, 54:165–187.

Grinshpun, S., Willeke, K., Kalatoor, S., and Baron, P. (1995). Development and Evaluation of an Aerosol Monitor with Low Wind Sensitivity and Uniform Filter Deposition. *J. Aerosol Sci.*, 26: S187–S188.

Hinds, W. C. (1999). *Aerosol Technology: Properties, Behavior, and Measurement of Airborne Particles*. Wiley.

Kalatoor, S., Grinshpun, S. A., Willeke, K., and Baron, P. (1995). New Aerosol Sampler with Low Wind Sensitivity and Good Filter Collection Uniformity. *Atmos. Environ.*, 29:1105–1112.

Kanerva, L., and Vaheri, E. (1993). Occupational Allergic Rhinitis in Finland. *Int. Arch. Occup. Environ. Health*, 64:565–568.

Kenny, L., Aitken, R., Baldwin, P., Beaumont, G., and Maynard, A. (1999). The Sampling Efficiency of Personal Inhalable Aerosol Samplers in Low Air Movement Environments. *J. Aerosol Sci.*, 30: 627–638.

Kenny, L., Aitken, R., Chalmers, C., Fabries, J., Gonzalez-Fernandez, E., Kromhout, H., Lidén, G., Mark, D., Riediger, G., and Prodi, V. (1997). A Collaborative European Study of Personal Inhalable Aerosol Sampler Performance. *Ann. Occup. Hyg.*, 41:135–153.

Kleinsasser, O., and Schroeder, H.-G. (1988). Adenocarcinomas of the Inner Nose After Exposure to Wood Dust. *Arch. Oto-Rhino-Laryngol.*, 245:1–15.

Kup, W. (1985). Industrial Nasal Problems. *Rhinology*, 23:99–100.

Labus, T. L., and Symons, E. P. (1972). Experimental Investigation of an Axisymmetric Free Jet with an Initially Uniform Velocity Profile. Report E-6801. National Aeronautics and Space Administration, Cleveland, OH.

Lidén, G., Juringe, L., and Gudmundsson, A. (2000). Workplace Validation of a Laboratory Evaluation Test of Samplers for Inhalable and "Total" Dust. *J. Aerosol Sci.*, 31:199–219.

Luce, D., Gerin, M., Morcet, J. F., Leclerc, A. (1997). Sinonasal Cancer and Occupational Exposure to Textile Dust. *Am. J. Ind. Med.*, 32:205–210.

Mark, D. and Vincent, J. H. (1986). A New Personal Sampler for Airborne Total Dust in Workplaces. *Ann. Occup. Hyg.*, 30:89–102.

Marshall, I., Mitchell, J., Griffiths, W. (1991). The Behaviour of Regular-Shaped Non-Spherical Particles in a TSI Aerodynamic Particle Sizer. *J. Aerosol Sci.*, 22:73–89.

McNaughton, K. and Sinclair, C. (1966). Submerged Jets in Short Cylindrical Flow Vessels. *J. Fluid Mech.*, 25:367–375.

Moscato, G., Vandenplas, O., Gerth Van Wijk, R., Malo, J., Quirce, S., Walusiak, J., Castano, R., De Groot, H., Folletti, I., Gautrin, D. (2008). Occupational Rhinitis. *Allergy*, 63:969–980.

O'Shaughnessy, P. T., and Raabe, O. G. (2003). A Comparison of Cascade Impactor Data Reduction Methods. *Aerosol Sci. Technol.*, 37:187–200.

Ogden, T. and Birkett, J. (1975). The Human Head as a Dust Sampler. *Inhaled Particles* 4:93.

Pesch, B., Pierl, C. B., Gebel, M., Gross, I., Becker, D., Johnen, G., Rihs, H.-P., Donhuijsen, K., Lepentsiotis, V., and Meier, M. (2008). Occupational Risks for Adenocarcinoma of the Nasal Cavity and Paranasal Sinuses in the German Wood Industry. *Occup. Environ. Med.*, 65:191–196.

Peters, T. M., Ott, D., and O'Shaughnessy, P. T. (2006). Comparison of the Grimm 1.108 and 1.109 Portable Aerosol Spectrometer to the TSI 3321 Aerodynamic Particle Sizer for Dry Particles. *Ann. Occup. Hyg.*, 50:843–850.

Rasband, W. *ImageJ 1.46r*, National Institute of Health.

Reynolds, A. (1962). Observations of a Liquid-Into-Liquid Jet. *J. Fluid Mech.*, 14:552–556.

Rushton, L., Hutchings, S. J., Fortunato, L., Young, C., Evans, G. S., Brown, T., Bevan, R., Slack, R., Holmes, P., and Bagga, S. (2012). Occupational Cancer Burden in Great Britain. *Br. J Cancer*, 107:S3–S7.

Schlichting, H., Gersten, K., and Gersten, K. (2000). *Boundary-Layer Theory*. Springer.

Slager, R. E., Poole, J. A., LeVan, T. D., Sandler, D. P., Alavanja, M. C., and Hoppin, J. A. (2009). Rhinitis Associated with Pesticide Exposure Among Commercial Pesticide Applicators in the Agricultural Health Study. *Occup. Environ. Med.*, 66:718–724.

Slavin, R. G. (2003). Occupational Rhinitis. *Ann. Allergy, Asthma Immunol.*, 90:2–6.

Slovak, A., and Hill, R. (1981). Laboratory Animal Allergy: A Clinical Survey of an Exposed Population. *Br. J Ind. Med.*, 38:38–41.

Soderholm, S. C. (1989). Proposed International Conventions for Particle Size-Selective Sampling. *Ann. Occup. Hyg.*, 33:301–320.

Spear, T. M., Werner, M. A., Bootland, J., Murray, E., Ramachandran, G., and Vincent, J. H. (1998). Assessment of Particle Size Distributions of Health-Relevant Aerosol Exposures of Primary Lead Smelter Workers. *Ann. Occup. Hyg.*, 42:73–80.

Straif, K., Benbrahim-Tallaa, L., Baan, R., Grosse, Y., Secretan, B., El Ghissassi, F., Bouvard, V., Guha, N., Freeman, C., and Galichet, L. (2009). A Review of Human Carcinogens—Part C: Metals, Arsenic, Dusts, and Fibres. *Lancet Oncol.*, 10:453–454.

Volckens, J., and Peters, T. M. (2005). Counting and Particle Transmission Efficiency of the Aerodynamic Particle Sizer. *J. Aerosol Sci.*, 36:1400–1408.

WHO (1995). Wood Dust, IARC Monographs Evaluation of Carcinogenic Risks to Humans.

Youlden, D. R., Cramb, S. M., Peters, S., Porceddu, S. V., Møller, H., Fritschi, L., and Baade, P. D. (2013). International Comparisons of the Incidence and Mortality of Sinonasal Cancer. *Cancer Epidemiol.*, 37:770–779.

Zuskin, E., Kanceljak, B., Pokrajac, D., Schachter, E., Witek, T. (1990). Respiratory Symptoms and Lung Function in Hemp Workers. *Br. J Ind. Med.*, 47:627–632.

Zuskin, E., Mustajbegovic, J., Schachter, E. N., Rienzi, N. (1993). Respiratory Symptoms and Ventilatory Capacity in Workers in a Vegetable Pickling and Mustard Production Facility. *Int. Arch. Occupat. Environ. Health*, 64:457–461.

Zuskin, E., Skuric, Z., Kanceljak, B., Pokrajac, D., Schachter, E. N., and Witek, T. J. (1988a). Respiratory Findings in Spice Factory Workers. *Arch. Environ. Health*, 43:335–339.

Zuskin, E., Skuric, Z., Kanceljak, B., Pokrajac, D., Schachter, E. N., and Witek, T. J. (1988b). Respiratory Symptoms and Lung Function in Furriers. *Am. J. Ind. Med.*, 14:189–196.